Hindawi
Mobile Information Systems
Volume 2022, Article ID 6299093, 10 pages
https://doi.org/10.1155/2022/6299093

Research Article

Analysis of Velocity Measurement for Transonic Projectiles in Indoor Long Ballistic Range

Rongli Cai,[1] Linqiu Tan ,[1] Rui Chen,[1] Quanmin Guo ,[2] and Liangliang Huang[1]

[1]*School of Optoelectronics Engineering, Xi'an Technological University, Xi'an 710021, China*
[2]*School of Electronics Information Engineering, Xi'an Technological University, Xi'an 710021, China*

Correspondence should be addressed to Linqiu Tan; tanlinqiu@xatu.edu.cn

Received 27 April 2022; Revised 25 June 2022; Accepted 1 August 2022; Published 23 August 2022

Academic Editor: Mian Ahmad Jan

The indoor one-kilometer projectile velocity measurement system cannot accurately identify the transonic projectile signal due to the interference signals generated by aerodynamics and other factors. To solve this problem, theoretical prediction of the projectile velocity at the transonic velocity measurement point is calculated by external ballistic numerical simulation technology based on the motion law of the center of projectile mass and the known measurement parameters of the indoor measurement system. In the measurement, a fast cross-correlation algorithm is used to process the projectile signals including interference signals and obtain velocity values at the measurement point. Then the theoretical prediction is used as the reference standard and the velocity with the smallest absolute value of the absolute error is selected as the desired measured value. A 5.8 mm rifle bullet is used to conduct an indoor one-kilometer live experiment. The results show that the relative errors between the measured value obtained by this method and the theoretical prediction are less than 1%, which eliminates the influence of interference signals and provides a new method for the accurate measurement of the transonic projectile velocity.

1. Introduction

External ballistics is a discipline that studies the motion laws, flight characteristics, and related phenomena of weapon projectiles in the air. As one of the important indicators, projectile velocity makes the range test one of the important links in the inspection of guns, cannons, ammunitions, and propellants [1–4]. Accurately measuring the multipoint velocity in the outer trajectory of the weapon system plays a vital role in the design of the projectile and the improvement of the battle effectiveness of the weapon system [5–7]. With the development of new weapon systems, the need for building an indoor full-trajectory test platform for light weapons has become increasingly urgent [8]. Due to poor test accuracy and lack of real-time performance and safety, early contact measuring devices such as paper targets, net targets, and wooden targets are being gradually eliminated. Although the existing photoelectric testing systems with intersecting detection areas are widely used in various shooting ranges, it is difficult to meet the requirements of high sensitivity and large-area velocity measurement at the same time [9, 10]. The indoor one-kilometer ballistic range velocity measurement system based on lens-type high-velocity small target velocity measurement technology fills the technical gap in this field [11]. However, in the actual test process, the projectile flies at supersonic or transonic velocity when its flying velocity is between 350 and 450 m/s. At this time, the projectile will generate shock waves under the action of aerodynamic force, which will cause the photodetector to generate false trigger signals and interference signals that are very similar to the projectile signal [12]. This prevents the signal processing equipment from accurately identifying the projectile signal, which results in the failure of full-trajectory velocity test. There is still no suitable method to solve the above problems due to the extremely high uncertainty in the generation of shock waves and the immature technology of full-trajectory velocimetry.

In this thesis, a new method is proposed to obtain the velocity of the transonic projectile accurately based on theoretical research, numerical simulation, and live

ammunition verification. It laid a solid foundation for the development of an indoor full-ballistic test platform for light weapons.

2. Configuration of the Velocity Measurement System

This research is based on the only indoor one-kilometer ballistic range velocity measurement system in the world. The schematic diagram of this system is shown in Figure 1. In order to achieve projectile velocity measurement in the entire trajectory, measurement stations are arranged at five predetermined positions: 200 m, 400 m, 600 m, 800 m, and 1000 m away from the muzzle, and the muzzle frame detector is used to detect the muzzle flare signal. A central control computer located in the main control room unifies all velocity measurement points through the network control. Each velocity measurement point is equipped with two L-shaped light sources, a set of velocity measurement devices with a photosensor, and a signal processing device. When the projectile passes through the two detection areas, the photoelectric receiving device will output the projectile signals. These signals are collected and preprocessed by the signal processing device. Then the data are transmitted to the terminal processing center for processing and the projectile flying velocity can be obtained. Therefore, the theoretical measurement of velocity can be realized at any two different measuring points within the range of 1 km.

In the actual test process using this method, several interference waveforms similar to the projectile signal will be collected at a certain velocity measurement point, as the projectile at this measurement point is in a transonic state. These waveforms will interfere with the extraction of real signals and cannot be effectively identified using the current equipment and technology.

3. Analysis of the Mechanism of Interference Signal

The lens-type photoelectric detection velocity measuring device is an instrument characterized by photoelectric conversion technology to detect the moment when a flying projectile reaches a specified position in space. Shock waves generated by the aerodynamic force of the projectile at a certain time during the flight will affect the change of the luminous flux obtained by the photoelectric conversion device. Therefore, when the projectile passes through the detection area, interference signals with a high degree of similarity to the projectile signal will be generated and the signal processing equipment cannot accurately identify the desired projectile signal.

3.1. Impact of Shock Waves on Light Propagation. In the field of aerodynamics, a high-velocity projectile compresses the surrounding air during the flight, and the interface formed between the compressed air and the surrounding undisturbed air is called a shock wave [13, 14]. The conical head of the projectile forms a cone wave with the trajectory as the axis and the apex at the warhead (i.e., Mach Cone), which is called the warhead wave. The airflow of the projectile tail is compressed strongly along the edge of the vortex-filled vortex to form the elastic wave. The warhead wave and the elastic wave are presented in Figure 2.

When the projectile velocity is less than 272 m/s, the air will be disturbed and propagates at the local sound velocity, which is greater than the projectile velocity. In this subsonic state, the distribution of the flow velocity and the pressure of the entire flow field is continuous and no shock wave is generated. When the flying velocity of the projectile is greater than 408 m/s, the projectile is in the supersonic phase. The gas will be compressed, and the pressure gradient of the projectile head will change. At this time, a warhead shock wave will be generated, the velocity of which is much lower than the projectile velocity. If the projectile velocity is between 272 m/s and 408 m/s, it is a transonic velocity of flight. At this time, there may be local shock waves around the warhead, which are less than, equal to, or greater than the sound velocity. As a result, the photoelectric detection device will recognize multiple trigger signals including the projectile signal [15]. The temperature, density, pressure, and refractive index of the compressed gas within the shock wave will change. The relationship between the refractive index and the density is

$$n = 1 + K_{\mathrm{GD}}\rho, \tag{1}$$

where K_{GD} is the conversion coefficient, which is a constant, and ρ is the gas density. After the gas density is determined, the change law of the refractive index can be known. The trajectory of the light can be determined by

$$\begin{aligned}\frac{\mathrm{d}}{\mathrm{d}x}\left(n\frac{\mathrm{d}r}{\mathrm{d}s}\right) &= \nabla n \\ &= i\frac{\partial n}{\partial x} + j\frac{\partial n}{\partial y} + k\frac{\partial n}{\partial z},\end{aligned} \tag{2}$$

where r is the position vector of the light trail, s is the light path, and $\nabla n = \mathrm{gradn}$ is the refractive index gradient, which reflects the law of light propagation in the refractive index gradient medium [16].

In order to facilitate light tracing and analyze the impact of shock waves on light propagation and luminous flux changes, it is assumed that the detection surface is perpendicular to the axis of the shock surface, the refractive index within the shock surface is a certain constant, and the refractive index of the uncompressed gas outside the shock surface is $n_0 = 1$. Figure 3 presents the geometric relationship between the incident light, the refracted light, the normal, and the shock wave cone. The incident plane is formed from the incident light AB, the normal BO, the refracted light BQ, and the shock cone. In order to find the direction and angle of the outgoing light, the first thing is to draw a normal line of the shock cone surface through the point Q and intersect the cone axis at $O2$. Then the exit plane can be determined by the normal line passing the point $O2$ and the line BQ, and the direction and angle of the outgoing light QR can be determined according to the law of refraction.

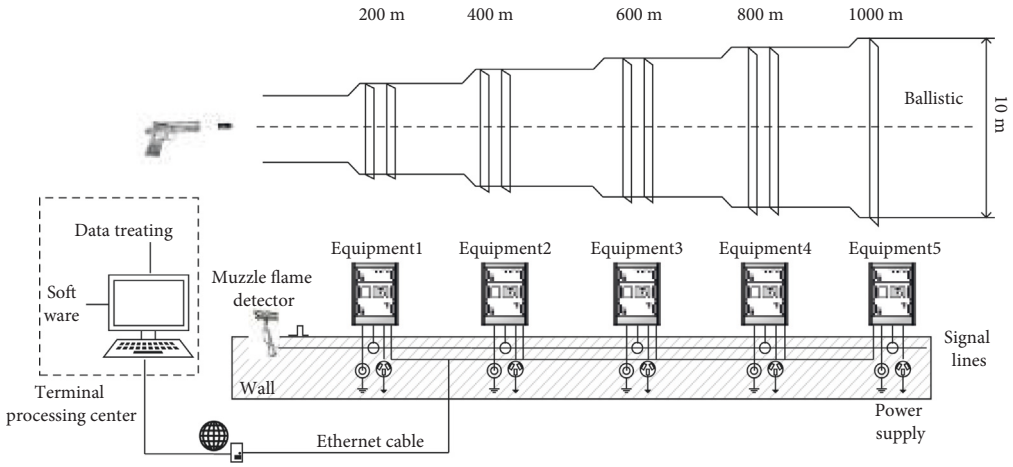

Figure 1: Schematic diagram of the indoor one-kilometer ballistic range velocity measurement system.

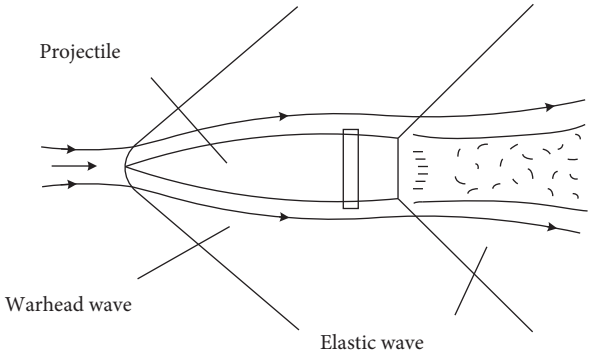

Figure 2: Schematic diagram of projectile shock waves.

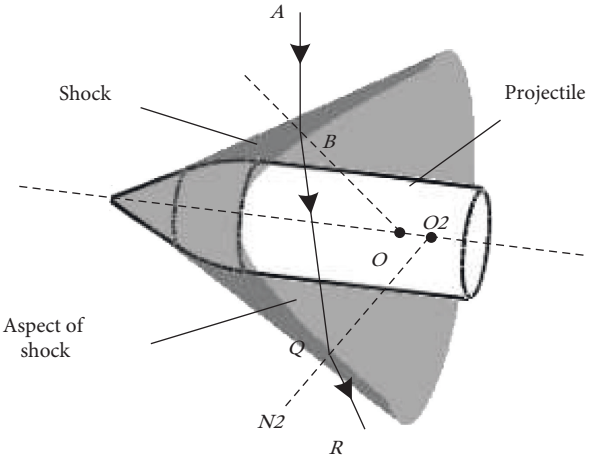

Figure 3: Relationship between incident light, refracted light, normal surface, and cone surface.

Figure 4 is a schematic diagram of the light propagation direction affected by shock waves when the projectile passes through the detection area.

The density, temperature, pressure, and refractive index in the shock surface will change due to the compression of the internal air [17, 18]. The change in air density before and after the shock wave causes the light to be refracted when passing through the space where the shock wave is located, and the light emitted by the light source deviates from the propagation track, so that part of the light beams cannot be normally irradiated on the predetermined photoelectric conversion device.

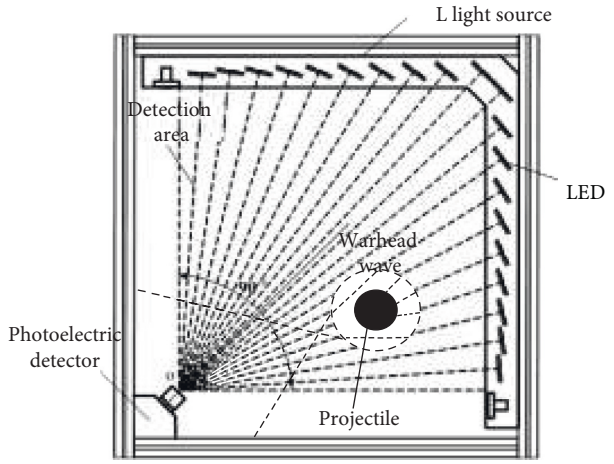

Figure 4: Schematic diagram of projectiles affected by shock waves.

3.2. The Generation Mechanism of Interference Signals. The indoor large-area photoelectric detection system consists of an optical lens, photosensitive components, and a signal processing circuit. Its output signal is determined by the amount of change in luminous flux caused by the projectile passing the detection area. Combining the photoelectric conversion principle of photosensitive components and the related theories of projectile passing through the detection area, the relationship between the change in luminous flux when the projectile passes through the detection area and the voltage variation of the signal processing circuit can be derived as

$$\Delta V(t) = \Delta\Phi \cdot \varepsilon \cdot \gamma \cdot R, \tag{3}$$

where $\Delta V(t)$ is the amount of voltage change, $\Delta\Phi$ is the amount of change in the luminous flux of the projectile passing through the detection area, ε is the luminous sensitivity of the photodetector, γ is the circuit gain, and R is the bias resistance of the photoelectric conversion circuit.

The schematic diagram of the lens-type photoelectric detection system is shown in Figure 5. Three lenses are spliced to form a wide-angle detection field of view. Each single lens and a slit diaphragm form a 30° fan-shaped detection field of view, and the three lenses are spliced into a 90° detection field of view.

Photosensitive components are composed of multiple photodiodes. A single photodiode equivalent circuit contains junction capacitance, bulk resistance, reverse bias resistance, and load resistance. Therefore, the larger the number of photodiodes connected in parallel in the circuit, the smaller the bias resistance and the larger the capacitance value of the signal processing circuit, thereby reducing the sensitivity and frequency response characteristics of the detector [19]. The impact of the shock wave on a single photosensitive device is minimal, but the superposition of interference signals generated by multiple photosensitive devices may produce interference signals that are very similar to normal projectile signals, making it difficult for the system to extract effective signal. Existing velocity measurement equipment and methods are difficult to process the signal generated in this case and further obtain the velocity value.

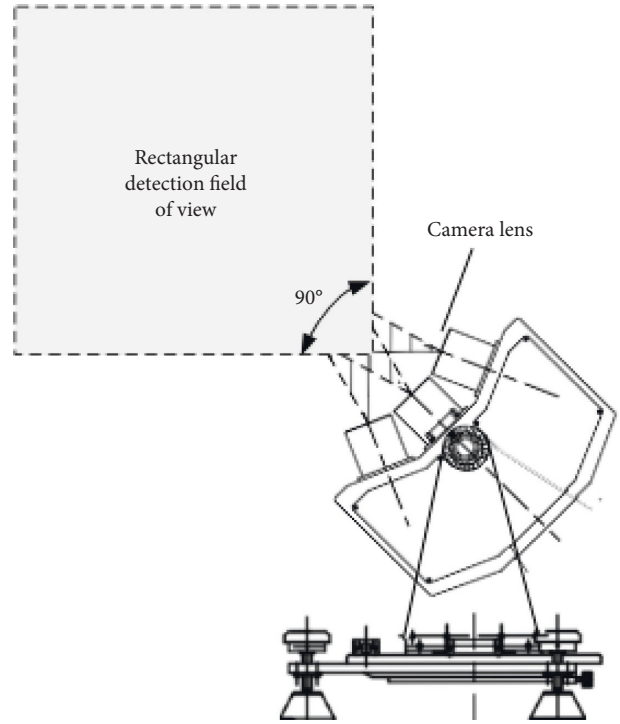

Figure 5: Schematic diagram of the lens-type photoelectric detection system.

4. Design and Verification of Signal Processing Algorithms

4.1. The Overall Program of Transonic Projectile Velocity Measurement. In order to solve the problem of inaccurate velocity measurement due to the failure of effective signal recognition of transonic projectiles, a simulation model is established based on the theory of external ballistics. The more realistic the initial input data, the more accurate the simulation results will be. Therefore, the theoretical calculation of the center of projectile mass motion equation is performed based on the parameters obtained in the indoor one-kilometer ballistic range velocity measurement system as initial values. The calculation results can provide a reliable reference value for the accurate measurement of transonic projectile velocity. The existence of shock waves makes unpredictable errors in velocity measurement. In order to ensure the accuracy and reliability of the velocity measurement, the characteristics of the projectile signal and the interference signal generation mechanism were analyzed. Then corresponding signal processing algorithms were designed to realize the measurement of transonic projectile velocity. The overall implementation plan is shown in Figure 6.

The signal processing algorithm is based on a fast cross-correlation algorithm and the transonic velocity measurement point signals are analyzed and processed. Then the velocity values generated by the projectile signal and shock wave interference signals can be obtained. Compared with the theoretical prediction obtained by the motion equation of the center of projectile mass, the velocity with the smallest absolute value of the absolute error is selected as the desired result.

4.2. Theoretical Simulation of External Ballistic Projectile Velocity. When studying the motion law of the center of projectile mass, generally in order to simplify the problem, the following assumptions need to be made: (1) The angle of attack δ is $\delta \equiv 0$ during the entire projectile movement. (2) The shape and mass distribution of the projectile are symmetrical about the longitudinal axis. (3) The surface of the Earth is a plane, the gravitational acceleration is constant, and the direction is vertical downward. (4) The Coriolis acceleration is zero. (5) The meteorological conditions are standard and there is no wind or rain.

Under the above assumptions, only gravity and air resistance act on the projectile [20], and the motion vector equation of the center of projectile mass is obtained:

$$\frac{dv}{dt} = a_x + g, \tag{4}$$

where a_x is the resistance acceleration and g is the gravity acceleration.

The motion equation of the center of projectile mass is usually studied in a Cartesian coordinate system with t as the independent variable in order to obtain its scalar equation. The horizontal component and the vertical component of velocity can be obtained by projecting in a rectangular coordinate system: $v_x = dx/dt = v\cos\theta$ (θ is the angle between the actual movement direction of the projectile and the x-axis), $vy = dy/dt = v\sin\theta$, and $v = (vx^2 + vy^2)^{1/2}$. The gravity acceleration g is in the negative direction of the y-axis, and the resistance acceleration a_x is in the opposite direction of velocity. Projecting both sides of (4) into the

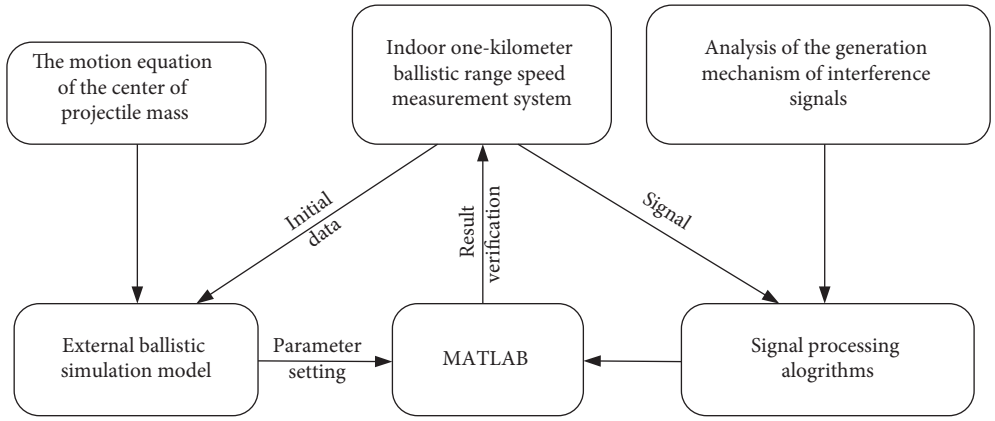

Figure 6: A block diagram of the overall solution for transonic projectile velocity measurement.

Cartesian coordinate system and adding the pressure change equation, we will get the center of mass motion equations in the Cartesian coordinate system:

$$\begin{cases} \dfrac{dv_x}{dt} = -cH(y)G(v)v_x, \\ \dfrac{dv_y}{dt} = -cH(y)G(v)v_y - g, \\ \dfrac{dy}{dt} = v_y, \\ \dfrac{dx}{dt} = v_x, \\ v = \sqrt{v_x^2 + v_y^2}, \end{cases} \tag{5}$$

where $H(y) = \rho/\rho_{oN} = (20000\text{-}y)/(20000 + y)$ is the air density function (ρ is the air density and ρ_{oN} is the standard air density, $y \le 10000$ m), $G(v) = F/v = 4.737 \times 10^{-4} C_{xoN}(Ma)$, v is the resistance function (Ma is the Mach number, C_{xoN} is the drag coefficient of the standard bomb), and $c = id^2/m \times 10^3$ is the ballistic coefficient (d is the warhead diameter, m is the mass, i is the elasticity coefficient).

The 5.8 mm rifle bullet is taken as the research object. The diameter of the warhead is 5.8 mm, the mass of the projectile is 12.63 g, and the full-trajectory length is 58.0 mm. The actual measured velocity of the projectile at the 200 m velocity point of one-kilometer ballistic range is taken as the initial value of the numerical simulation. Assuming that the projectile's flight attack angle is zero at this time, changes in horizontal displacement and projectile velocity as a function of time under the conditions of resistance and no resistance are shown, respectively, in Figures 7 and 8.

Combined with Figures 7 and 8, the comparison of experimental data gained by the one-kilometer ballistic range velocity measurement system with the theoretical prediction obtained by the above numerical simulation method is shown in Figure 9.

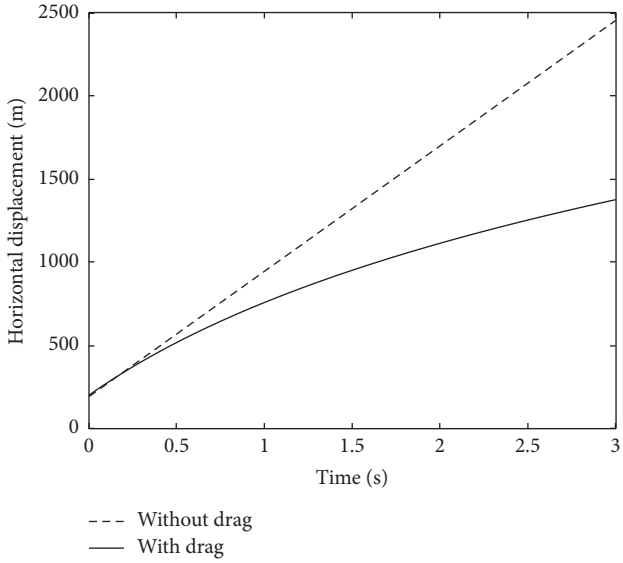

Figure 7: Change in horizontal displacement as a function of time.

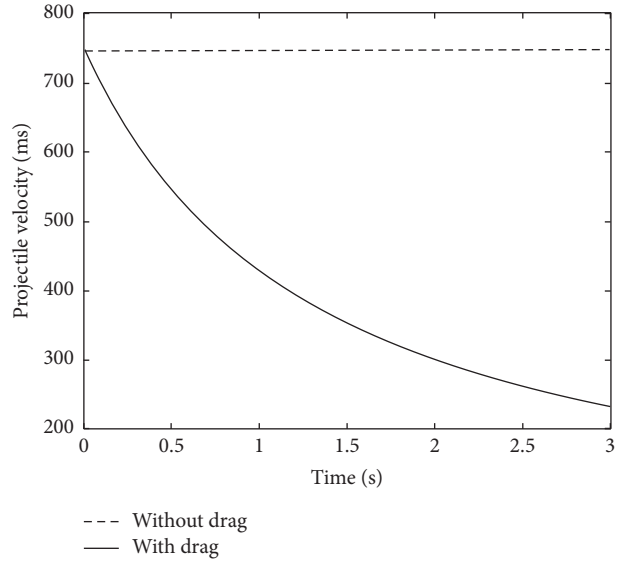

Figure 8: Change in projectile velocity as a function of time.

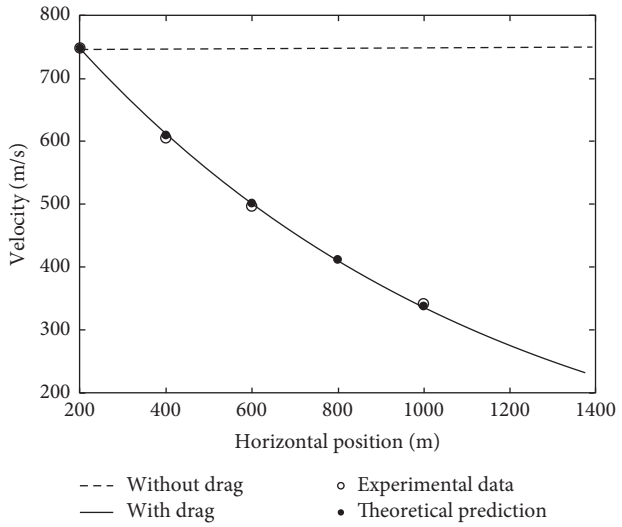

Figure 9: Comparison of experimental data with the theoretical prediction.

It can be seen from Figure 9 that for a 5.8 mm rifle projectile, the projectile at 800 m velocity measurement point is in a transonic state, and the signal processing equipment cannot accurately obtain the projectile velocity at this point. The relative errors between the experimental data and the theoretical prediction are shown in Table 1.

It can be seen from Table 1 that the relative errors between the experimental data and the theoretical prediction at velocity measurement points except for 800 m velocity measurement point are all not more than 1%.

4.3. Algorithm Verification and Result Analysis. A fast cross-correlation algorithm can be used to analyze and process the projectile signal at the transonic velocity measurement point. However, the length of the two sequences to be calculated must be equal and be an integer power of two if the fast cross-correlation algorithm based on fast Fourier transform (FFT) and inverse fast Fourier transform (IFFT) is used to calculate the delay of the two signals [21, 22]. If the above conditions are not met, aliasing distortion will occur, and zeros can be added to prevent aliasing distortion. The calculation formula for fast cross-correlation between two sequences of equal length $x(n)$ and $y(n)$ is shown as

$$R_{xy}(n) = \sum_{k=0}^{N-1}\left[\frac{1}{N}R_{\mathrm{xy}}(k)W_N^{-\mathrm{nk}}\right] = \frac{1}{N}\{\mathrm{FFT}[X^*(k)\cdot Y(k)]\}^*, \quad (6)$$

where N is the sequence length and k is an integer. The process of signal processing algorithm is shown in Figure 10.

First, two random signals $x(t)$ and $y(t)$ are sampled and preprocessed to obtain the sequence $x(n)$ and $y(n)$ of length m. Second, the period $N \geq 2m\text{-}1$, where $m = 2h$ (h is an integer) is selected; if the lengths of the two signals are inconsistent, zeros are added after the shorter signal to obtain the sequence $x'(n)$ and $y'(n)$ of length N. Third, $x'(n)$ and $y'(n)$ are performed by FFT, respectively, $X(k) = \mathrm{FFT}[x'(n)]$, $Y(k) = \mathrm{FFT}[y'(n)]$. Fourth, $X*(k)$ is obtained by taking the conjugate of $X(k)$, and then $R_{xy}(k) = X*(k)\cdot Y(k)$ can be obtained. Lastly, IFFT processing is performed on $R_{\mathrm{xy}}(k)$ to obtain the cross-correlation processing result of the two signals, $R_{\mathrm{xy}}(\tau) = \mathrm{IFFT}[X*(k)\cdot Y(k)]$.

Table 1: Relative errors between the experimental data and the theoretical prediction.

Horizontal displacement (m)	Experimental data (m/s)	Theoretical prediction (m/s)	Relative error
200	748.6	748.6	0
400	605.7	610.3	0.7%
600	497.3	502.2	0.9%
800	—	412.5	—
1000	342.1	338.5	1%

In order to obtain the transit time τ_0 (represented by an integer multiple q of the sampling interval τ_p), the peak search method is used to find the maximum value of $R_{\mathrm{xy}}(\tau)$. The distance L between the front and rear detection areas of each velocity measurement point is 5 m, and the corresponding velocity value V can be obtained according to the transit time: $V = L/\tau_0 = L/(q\tau_p)$.

4.3.1. Signal Processing Algorithm. The feasibility of this method is verified by taking the 5.8 mm rifle projectile signal as an example. Assuming that the sampling frequency of the velocity measurement system is 1 MHz, the experimental data at the 200 m velocity measurement point and the 800 m transonic velocity measurement point are processed, respectively. The processing results are shown in Figures 11–13. The abscissa is the number of samples, and the ordinate represents the amplitude. Figure 11(a) is the projectile signal collected at the 200 m measurement point, and Figure 11(b) is the algorithm processing results processed by the cross-correlation function (xcorr) and the fast cross-correlation algorithm, respectively. The projectile at the 200 m measurement point is not in a transonic state, so there is no interference signal in the original signals. However, at the 800 m measurement point, the projectile is in a transonic state, so the original signals will contain interference signals. The projectile signals with one interference signal and with two interference signals at 800 m measurement point are shown in Figures 12(a) and 13(a), respectively. The corresponding processing results are shown in Figures 12(b) and 13(b).

It can be seen that there is not only one algorithm processing result in Figures 12(b) and 13(b), but only one result is the real projectile signal processing result. Furthermore, the more interference signals, the more algorithm processing results. It can also be seen that the processing results obtained by the two algorithms (xcorr function and fast cross-correlation algorithm) are the same, but the algorithm execution times are different. Under the same conditions, the processing time of the two algorithms are shown in Table 2.

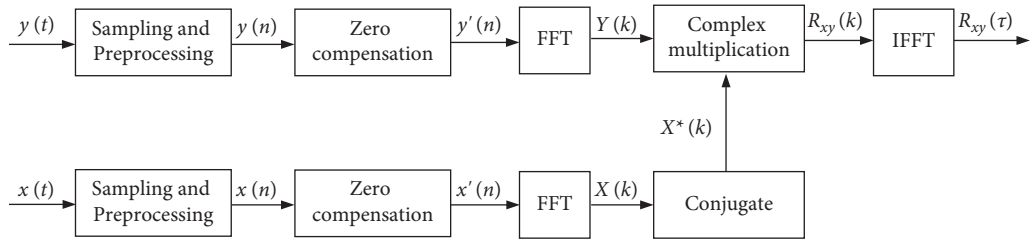

Figure 10: The process of signal processing algorithm.

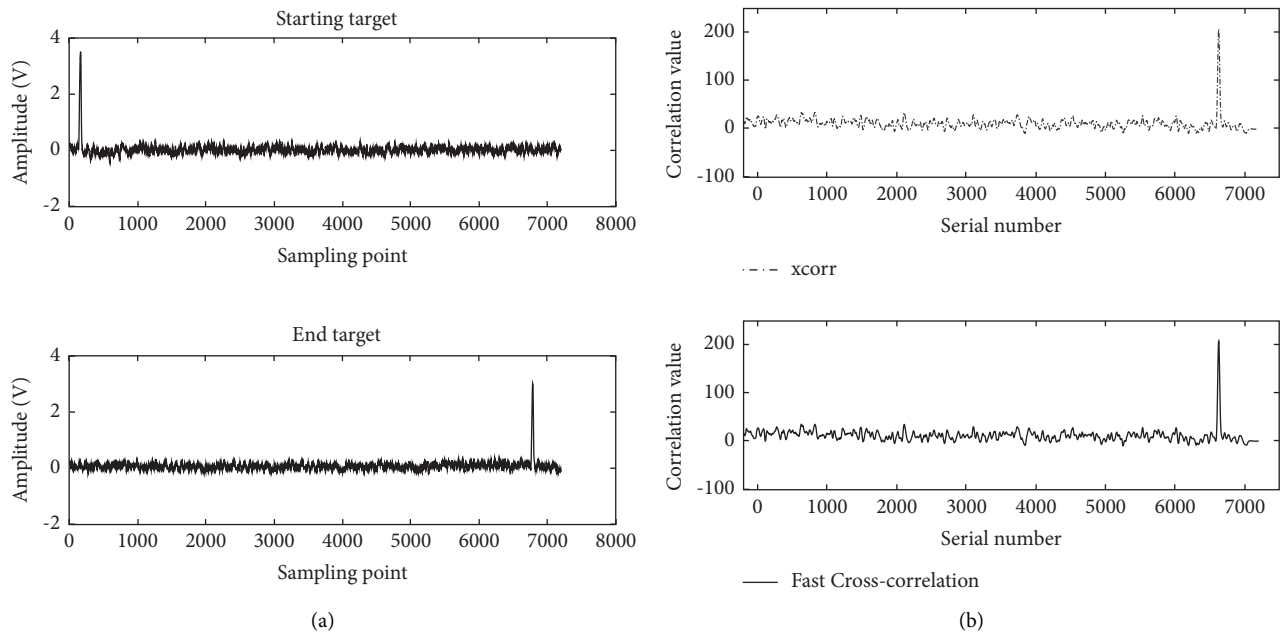

Figure 11: Collected projectile signals and the algorithm processing results at 200 m measurement point: (a) original collected signals; (b) algorithm processing results.

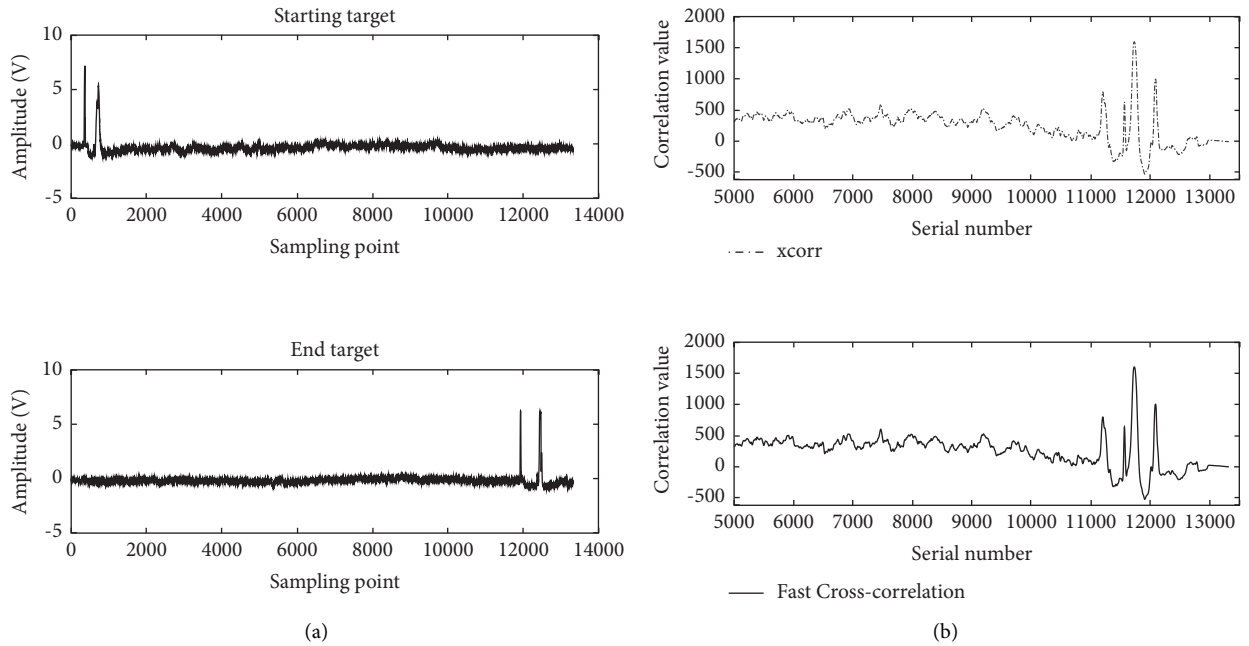

Figure 12: Collected projectile signals including one interference signal and the algorithm processing results at 800 m measurement point: (a) original collected signals; (b) algorithm processing results.

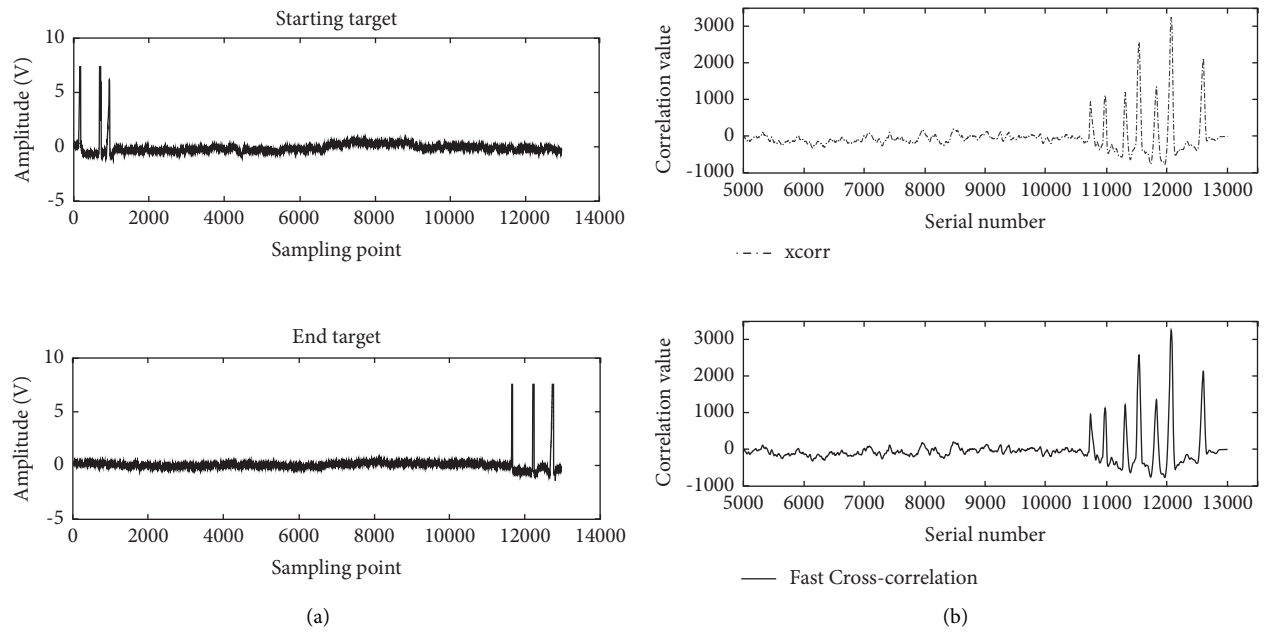

Figure 13: Collected projectile signals including two interference signals and the algorithm processing results at 800 m measurement point: (a) original collected signals; (b) algorithm processing results.

Clearly, in the three different situations, for the same data, the execution time of the fast cross-correlation algorithm is nearly 1 order of magnitude shorter than the xcorr function. Therefore, selection of the fast cross-correlation algorithm can improve processing efficiency.

4.3.2. Analysis of Processed Results. Corresponding to the two cases in Figures 12 and 13, the velocity values processed by the fast cross-correlation algorithm and the theoretical values obtained by the external ballistic numerical simulation at 800 m velocity measurement point are shown in Figure 14.

The true velocity value of the transonic projectile is included in the velocity values after the fast cross-correlation processing. To obtain the true velocity value accurately, it is necessary to compare them with the theoretical prediction. The velocity value with the smallest absolute value of the absolute error is the desired result. Table 3 shows the algorithm processing results of 5.8 mm projectile velocities at 800 m velocity measurement point in two cases as shown in Figures 12 and 13.

It can be seen from Table 3 that at 800 m velocity measurement point, whether there is one interference signal or two interference signals, the relative errors between the transonic projectile velocities obtained by the above method and the theoretical value are less than 1%. This result is within the same range as the relative errors measured at other velocity measurement points without shock wave interferences (such as 200 m, 400 m, and 1000 m velocity measurement points) in Table 1, and both are not more than 1%. It shows that the results obtained by the fast cross-correlation algorithm can give the transonic projectile velocity accurately within the allowable range of the relative error.

Table 2: Comparison of the execution time of the two algorithms.

	Processing time (s)	
	xcorr function (s)	Fast cross-correlation (s)
No interference signal	0.031962	0.0051212
One interference signal	0.035449	0.0072062
Two interference signals	0.037335	0.0079811

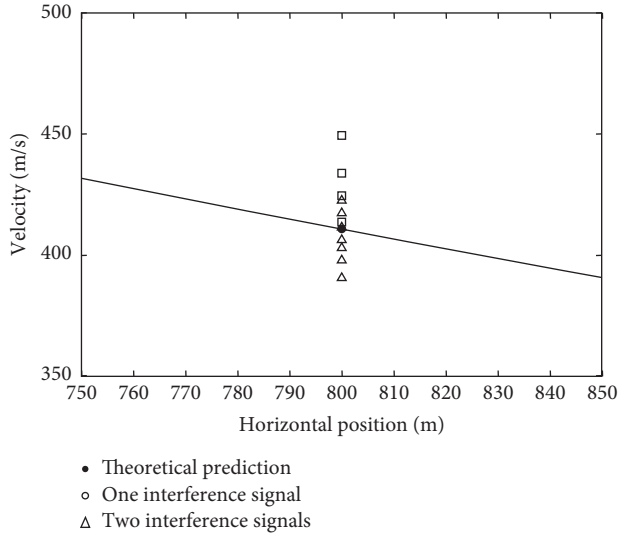

Figure 14: The velocity values processed by the fast cross-correlation algorithm and the theoretical values in two interference situations at 800 m velocity measurement point.

Table 3: Algorithm processing results in two cases.

Original signal	Algorithm processing results (m/s)	Theoretical prediction (m/s)	Desired value (m/s)	Relative error (%)
Case 1: at 800 m velocity measurement point with one interference signal	449.4, 433.8, 424.5, 414.6	412.5	414.6	0.51
Case 2: at 800 m velocity measurement point with two interference signals	422.5, 417.3, 413.1, 408.6, 402.9, 397.8, 390.5	412.5	413.1	0.15

5. Conclusion

Based on the indoor one-kilometer ballistic range velocity measurement system, a theoretical study and live ammunition test were carried out on the whole ballistic velocity measurement. In particular, the external ballistic numerical simulation technology and fast cross-correlation algorithm are combined to obtain the flight velocity of the transonic projectile. Using 5.8 mm projectiles as the research objects, the results show that the relative errors between the transonic projectile velocities obtained by the above method and the theoretical prediction are not more than 1%. It avoids the failure of the entire system test due to the impact of shock wave interference on transonic projectile signal, and as this method is based on photoelectric principle, it only requires that the projectile is opaque, which is basically not limited by the projectile material. It provides a new method for measuring the projectile velocity of full trajectory.

Data Availability

No data were used to support this study.

Conflicts of Interest

The authors declare that there are no conflicts of interest regarding the publication of this article.

Acknowledgments

This work was supported by the Young Scientists Fund of the National Natural Science Foundation of China (grant no. 61905187); the Scientific Research Plan Projects of Shaanxi Education Department (grant no. 20JK0692); and the Shaanxi Provincial Key Research and Development Program (grant no. 2019GY-094).

References

[1] J. F. Moxnes, A. K. Prytz, O. Frøyland, S. Skriudalen, S. Børve, and G. Odegardstuen, "Strain rate dependency and fragmentation pattern of expanding warheads," *Defence Technology*, vol. 11, pp. 1–9, 2015.

[2] Y. Zhang, Z. D. Wang, Z. Q. Zha, and L. F. Bai, "Research and implementation of velocity and position measurement method of projectile," *Proceedings of SPIE*, vol. 8908, Article ID 89081k, 17 pages, 2013.

[3] E. Musa and M. Demirer, "Laser-based light barrier having a rectangular detection area," *Optics and Lasers in Engineering*, vol. 48, no. 4, pp. 435–440, 2010.

[4] R. Chen, D. Chen, B. Ji, and J Ni, "Inversion method of the key structure parameters of light screen array measurement system using genetic algorithm," *Optik*, vol. 206, Article ID 164064, 2020.

[5] J. C. Zhang, T. L. Zhang, and Z. Y. Cai, "A method of initial velocity measurement for rocket projectile," *MATEC Web of Conferences*, vol. 128, pp. 04012–04302, 2017.

[6] R. Chen, R. Cai, and B. Ji, "Projectile flight parameters measurement method based on the spatial distribution of light-screen thickness," *Measurement*, vol. 195, Article ID 111143, 2022.

[7] G. S. Gill and A. Kumar, "Velocity measurement system for small caliber projectiles," *Lecture Notes in Engineering and Computer Science*, vol. 2170, no. 1, pp. 2–4, 2008.

[8] F. Q. Chao, J. Y. Du, G. C. Mu, Y. T. Qi, and G. H. Zhao, "Present situation and development trend of intelligent ammunition test measuring in range," *Fire Control and Command Control*, vol. 39, no. 08, pp. 181–184, 2014.

[9] Z. C. Wu and X. L. Zhang, "On-sate calibration method of target distance of the sky screen target velocity measuring system," *Optik*, vol. 178, pp. 483–487, 2019.

[10] R. L. Cai, J. P. Ni, and H. Tian, "A new design used in optical screen for measuring velocity of bullets," *Optical Technique*, vol. 32, no. 5, pp. 790–792, 2006.

[11] 高. Gao Fen, 倪. Ni Jinping, 田. Tian Hui, 董. Dong Tao, and 冯. Feng Bin, "Design on the large sensor area light screen for velocity measurement of the flying projectile indoor," *Optical Technique*, vol. 38, no. 2, pp. 175–179, 2012.

[12] A. Kumar, H. S. Panda, T. K. Biswal, and R. Appavuraj, "Flow around a conical nose with rounded tail projectile for subsonic, transonic, and supersonic flow regimes: a numerical study," *Defence Science Journal*, vol. 64, no. 6, pp. 509–516, 2014.

[13] J. Sahu, "Numerical computations of transonic critical aerodynamic behavior," *AIAA Journal*, vol. 28, no. 5, pp. 807–816, 1990.

[14] A. Peraiah, "Flux vector splitting of the inviscid radiation gas dynamic equations," *Kodaikanal Observatory Bulletins*, vol. 3, pp. 49–56, 1980.

[15] D. H. Feng, P. Sha, Z. Y. Tian, and H. Li, "Method of ray tracing through shock wave flow field," *Journal of National University of Defense Technology*, vol. 32, no. 1, pp. 6–10, 2010.

[16] X. D. Gao, X. H. Ji, and X. S. Wu, "Numerical studies of the flow field over a low-drag and long-range projectile by implicit TVD scheme," *Acta Armamentarii*, vol. 23, no. 2, pp. 180–183, 2002.

[17] Z. Q. Zhang, L. Wang, D. Xu, J. F. Luo, and Y. F. Zhang, "Analysis of projectile shock wave's influence on measure of

laser screen," *Optical Technique*, vol. 34, no. S1, pp. 203–205, 2008.

[18] K. Klimaszewski and T. W. Sederberg, "Faster ray tracing using adaptive grids," *IEEE Computer Graphics and Applications*, vol. 17, no. 1, pp. 42–51, 1997.

[19] W. Wang, K. Qu, X. X. Zhang, and Y. Guo, "A photodiode signal conditioning circuit for projectile velocity measurement," in *Proceedings of the International Conference on Automatic Control and Artificial Intelligence*, pp. 255–257, IEEE, Xiamen, March 2012.

[20] Z. P. Hang, *Exterior Ballistics of Projectiles and Rockets*, pp. 80–120, Beijing Institute of Technology Press, Beijing, China, 2008.

[21] H. C. Yan and W. Y. Liu, "Design of time difference of arrival estimation system based on fast cross correlation," in *Proceedings of the 2010 2nd International Conference on Future Computer and Communication*, pp. V2V464–V2466, IEEE, Wuhan, China, May 2010.

[22] X. L. Yang and X. B. Huang, "The influence factors and improvement measures for accuracy of correlation velocity measurement," *Applied Mechanics and Materials*, vol. 152-154, pp. 1118–1121, 2012.